IEEE Photonics Journal
An IEEE Photonics Society Publication

Invited Paper

Small-Signal Theory and Design of Traveling-Wave Semiconductor Cascade Lasers

Volume 2, Number 2, April 2010

H. Hashim, Member, IEEE
S. Iezekiel, Senior Member, IEEE

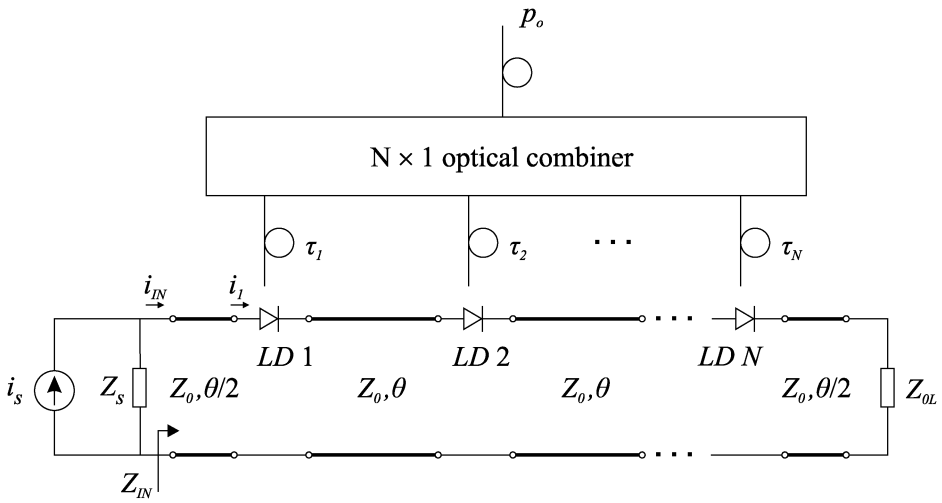

DOI: 10.1109/JPHOT.2010.2044500
1943-0655/$26.00 ©2010 IEEE

Small-Signal Theory and Design of Traveling-Wave Semiconductor Cascade Lasers

H. Hashim,[1] ***Member, IEEE*****, and S. Iezekiel,**[2] ***Senior Member, IEEE***

(Invited Paper)

[1]Department of Electrical and Communication Engineering, Institut Teknologi Brunei, Tungku Link BE1410, Brunei
[2]Department of Electrical and Computer Engineering, University of Cyprus, Nicosia 1678, Cyprus

DOI: 10.1109/JPHOT.2010.2044500

Manuscript received January 18, 2010; revised February 16, 2010 and February 19, 2010. First published Online February 25, 2010. Current version published March 23, 2010. Corresponding author: S. Iezekiel (e-mail: s.iezekiel@ieee.org).

Abstract: Traveling-wave semiconductor cascade lasers (TWSCLs) are a form of series cascade laser (SCL) in which series-connected laser diodes are interconnected with commensurate transmission lines to create a periodically loaded structure. The inclusion of transmission line segments allows broadband impedance matching in addition to preserving the link gain improvements of conventional SCLs. This paper describes the small-signal analysis of TWSCLs using both transmission line theory and Bloch waves. The latter technique is then applied to a study of how transmission line and laser diode parameters affect both the return loss and gain–bandwidth product of TWSCLs.

Index Terms: Semiconductor laser arrays, traveling wave devices, optical modulation.

1. Introduction

Analog fiber-optic links for the transmission of microwave signals in the optical domain offer potentially huge bandwidths and low loss compared with traditional microwave transmission media such as coaxial cable [1]–[5]. However, in order to make a meaningful comparison between optical fiber and microwave transmission media, one must also account for the electro-optic (E/O) and optoelectronic conversion (O/E) processes at either end of an analog fiber-optic link. The overall microwave fiber-optic link loss can be several decibels, due primarily to poor E/O and O/E conversion efficiency. Inclusion of active optoelectronic devices also leads to noise and nonlinearity. Thus, a link will be specified not only in terms of small-signal parameters such as return loss and link gain but noise figure and spur-free dynamic range as well. Techniques to improve one or more of these parameters revolve around choices of modulation technique, link architecture, or device type [6].

In terms of modulation format, coherent techniques offer improved receiver sensitivity (and hence link length) but require complex photoreceivers [7]. Although monolithic integration may offer a future path to low-cost coherent microwave fiber-optic links [8], intensity modulation/direct detection (IM/DD) schemes predominate for now. External modulators offer superior bandwidths and chirp-free operation for IM/DD links. However, directly modulated laser diodes (LDs) are a cheaper alternative to external modulation, and this consideration can be important in applications such as distributed antenna systems. Moreover, the use of optical injection locking has resulted in modulation bandwidth enhancement up to 80 GHz for vertical cavity surface emitting lasers [9].

Unlike external modulation, for which an increase in continuous wave optical power will improve link gain, in a directly modulated link the LD slope efficiency constrains the E/O contribution to link gain. Specifically, the differential quantum efficiency (DQE) cannot exceed 100%. However, if several LDs are cascaded in series and their outputs combined coherently into a single optical waveguide or fiber, then a DQE in excess of unity is possible [10]–[25]. The term "semiconductor cascade laser" (SCL) has been coined for such structures [17], and cascades using discrete devices [16] and monolithic implementations have been reported [14]. The SCL makes it possible to have microwave fiber-optic links with intrinsic gain without any consideration to impedance matching or use of amplification. In principle, for a series cascade of N LD segments feeding into a single waveguide, the SCL's contribution to microwave link gain scales by N^2 [26]. In practice, this scaling will be limited by a number of factors. The impedance of an SCL will increase as N increases; in the case of the segmented lasers in [21], it scales quadratically, thus placing an upper limit on the DQE should a 50-Ω match be desired (which at microwave frequencies, it is, in order to eliminate mismatch reflections). Impedance scaling can also adversely affect the SCL bandwidth, especially in cascades using discrete LDs, for which increased parasitic roll-off is observed [16].

Much of the work in SCLs is based on lumped models [26]. Given that the length of some monolithic SCLs tends to be larger than that of single laser chips, it might be anticipated that distributed microwave effects will arise. Even in single LDs, it has been shown that distributed effects occur, leading to loss and phase shifts along the length of the device [27] (although it was argued in [28] that this only degrades the bandwidth if a device is voltage driven). However, there is little work on the analysis of distributed effects in SCLs.

Recent work has shown how traveling-wave effects may be used to improve the return loss of SCLs without sacrificing the current recycling phenomenon [29], [30]. The resulting structure is termed a traveling-wave SCL (TWSCL). The TWSCL is a series connection of LDs in which lengths of transmission line (Z_0, θ) separate the LDs to constitute a traveling-wave circuit that can improve the input match while maintaining the gain inherent in SCLs. The impedance scaling that occurs in SCLs is mitigated by the distributed structure, analogous to the capacitance distribution effect in a traveling-wave amplifier. This, in principle, allows longer cascades and, therefore, higher gain.

Both the small-signal [29] and large-signal [30] performance of TWSCLs (fabricated in hybrid form) have been reported and indicate that improvements in link gain and reduction of intermodulation distortion are possible compared to a single resistively matched laser, for example. However, the detailed theory of such structures has not been discussed. The aim of this paper is to describe small-signal models of TWSCLs and their use in optimizing performance parameters such as gain–bandwidth product (GBP). This design approach has been used to realize the structures reported in [29] and [30].

2. Traveling-Wave Semiconductor Cascade Lasers

The topology of a TWSCL is shown in Fig. 1(a). It consists of N identical LDs in series with interconnecting transmission lines of electrical length θ and characteristic impedance Z_0. For simplicity, the biasing network is not shown. Although the TWSCL in Fig. 1(a) uses optical fiber pigtailed LDs, this can be abstracted as optical channels which may also be implemented using free-space optics or planar optical waveguides. Light from the LDs is collected in an $N \times 1$ optical combiner leading to an optical output power p_o, which is modulated at microwave frequencies. (In [29] and [30], a WDM fiber coupler was used in order to minimize optical losses.) It is necessary to compensate for the differing signal paths from individual LDs in order to improve the bandwidth.

In our analysis of the TWSCL, a small-signal equivalent circuit model of the intrinsic LD is used [31], and it is assumed that i) the LDs are biased well above threshold; ii) stimulated emission is dominant, and spontaneous emission contributions can be ignored [which simplifies the circuit model to a parallel RLC circuit as in Fig. 1(b)]; iii) only intensity modulation takes place (intensity modulation-to-frequency modulation effects are ignored); iv) the LDs are lumped, transmission lines are lossless, and chip parasitics are neglected; and v) line lengths are assumed to be short enough

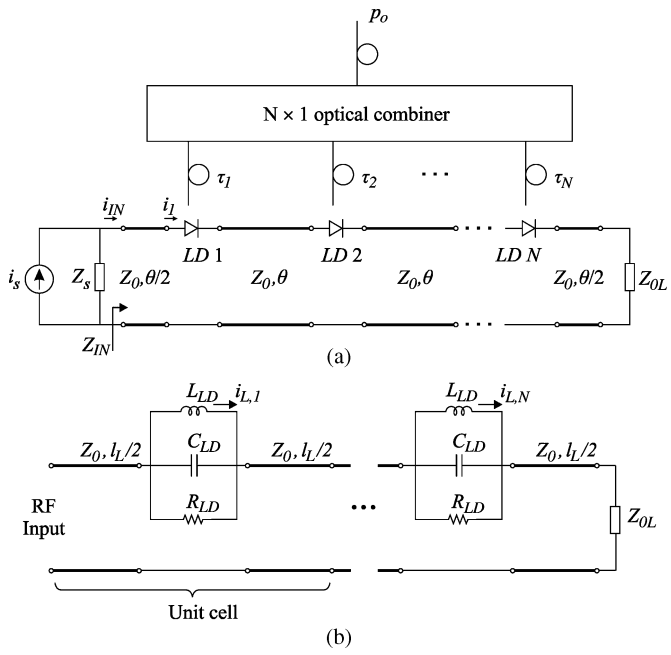

Fig. 1. (a) Traveling-wave series cascade of N laser diodes. (b) Distributed circuit of a TWSCL.

so that the distributed structure can be represented by a differential equivalent circuit. For convenience the anode of the LD is arbitrarily designated as port one and the cathode port two. The anode may also be referred to as the "p-side" and the cathode as the "n-side" of the LD.

Referring to Fig. 1(a), let the terminal current entering port one of LD 1 be i_1. Apart from the first LD, the amplitude of the current wave incident on (reflected from) port one of the nth LD is identically equal to the amplitude of the current wave reflected from (incident on) port two of the $(n-1)$th LD, since the transmission lines are lossless. Thus, the amplitude of the terminal current entering port one of the nth LD is equal to the amplitude of the current leaving port two of the $(n-1)$th LD and, hence, equal to $|i_1|$. Since the electrical length of the transmission line between adjacent LDs is θ, the terminal current entering port one of the nth LD is given by

$$i_n(j\omega) = i_1(j\omega)e^{-j(n-1)\theta} \tag{1}$$

where $1 \leq n \leq N$, and n is a positive integer. Using this result, the current through the equivalent circuit inductor $i_{L,n}$ of the nth LD can be expressed as

$$i_{L,n}(j\omega) = \frac{1}{1 - \omega^2 L_{\mathrm{LD}} C_{\mathrm{LD}} + j\omega L_{\mathrm{LD}}/R_{\mathrm{LD}}} i_n(j\omega). \tag{2}$$

This current in turn is proportional to the emitted photon density [32] and, hence, the small-signal variations in the optical power produced by the LD. Thus, the modulated optical output power from the nth LD is

$$p_{o,n}(j\omega) = \sigma i_{L,n}(j\omega) \tag{3}$$

where σ is a constant of proportionality with units of W/A, which is a measure of the electron–photon conversion efficiency. Hence, it is related to the DQE of the LD. While realizing that modulated optical power is a scalar quantity, the use of phasor notation is a useful mathematical construct for looking at the impact of phase shifts (such as those due to electrical delays and incoherent optical delays) in the

sinusoidal regime. This approach is common practice in the analysis of directly modulated LDs [32]. Substituting (2) into (3) and re-arranging yields the LD intensity modulation transfer function

$$H_{\mathrm{LD}}(j\omega) = \frac{p_{o,n}(j\omega)}{i_n(j\omega)} = \sigma \frac{\omega_{\mathrm{LD}}^2}{\omega_{\mathrm{LD}}^2 - \omega^2 + j\omega\gamma_{\mathrm{LD}}} \tag{4}$$

where $\omega_{\mathrm{LD}} = 1/\sqrt{(L_{\mathrm{LD}}C_{\mathrm{LD}})}$ is the LD resonant frequency, and $\gamma_{\mathrm{LD}} = 1/(R_{\mathrm{LD}}C_{\mathrm{LD}})$ is the damping factor of the modulation response. Using (1), the modulated output power for the nth LD is

$$p_{o,n}(j\omega) = H_{\mathrm{LD}}(j\omega) i_1(j\omega) e^{-j(n-1)\theta}. \tag{5}$$

Hence, the total modulated optical power at the output of the combiner is

$$p_o(j\omega) = H_{\mathrm{LD}}(j\omega) i_1(j\omega) e^{j\theta} \sum_{n=1}^{N} e^{-jn\theta} e^{-j\omega\tau_n} \tag{6}$$

where τ_n is the optical delay from the nth LD output to the input of the combiner. The second factor in the summation is due to propagation along the optical path from the LD to the combiner input. Since it is assumed that we are operating in the incoherent optical regime and that each LD is in essence a separate emitter, the summation applies to optical powers rather than the associated electric fields. In this respect the optical side of the TWSCL shares similarities with incoherent optical delay line structures used for filtering of modulated optical signals [33], in which it is assumed that the optical delays are much larger than the coherence length of the optical source. Equation (6) does not explicitly include losses due to the optical combiner; in our experimental work [29], [30], we have used WDM multiplexing in order to minimize optical losses.

From (6), a general expression for the transfer function of the TWSCL can be obtained as follows. Assuming negligible reflected waves in the first section of the TWSCL implies that $i_1(j\omega) = i_{\mathrm{IN}}(j\omega)e^{-j\theta/2}$. Expressing the input current i_{IN} in terms of the impedance seen by the source yields the desired transfer function

$$H_L(j\omega) = \frac{p_o(j\omega)}{i_s(j\omega)} = \frac{Z_s}{Z_s + Z_{\mathrm{IN}}(j\omega)} \cdot H_{\mathrm{LD}}(j\omega) e^{j\theta/2} \sum_{n=1}^{N} e^{-jn\theta} e^{-j\omega\tau_n}. \tag{7}$$

A study of the individual terms in (7) allows one to identify factors which affect the response of the TWSCL, namely input matching, modulation bandwidth and DQE of the LDs and the signal combining method, where the latter is described by the summation term. Now consider two cases for the combining scheme: (a) The optical path lengths are tailored so that the overall signal delays from the TWSCL input to the combiner input are identical, and (b) the optical path lengths are identical (but incoherent optical summation is still assumed). In the first case the magnitude of the summation reduces to N, the number of LDs in the TWSCL. Hence, it can be seen from the magnitude of the transfer function that the modulation response of a LD is enhanced by a factor of N. In the second case let the optical path delay be τ_o so that the factor $e^{-j\omega\tau_0}$ can be taken out of the summation. The latter is then the sum of a complex geometric sequence, the magnitude of which can be expressed as

$$\left| \sum_{n=1}^{N} e^{-jn\theta} \right| = \left| e^{-j\theta} \frac{1 - e^{-j\theta N}}{1 - e^{-j\theta}} \right| = \sqrt{\frac{1 - \cos\theta N}{1 - \cos\theta}}. \tag{8}$$

The above expression plays an important role in the transfer function of the TWSCL when the optical paths are identical and is plotted in Fig. 2 against the electrical length of the TWSCL unit cell for various values of N. Note that when $N = 1$, (8) is unity and the transfer function of the TWSCL simplifies to the modulation response of a LD as expected. From the figure, it can be seen that the

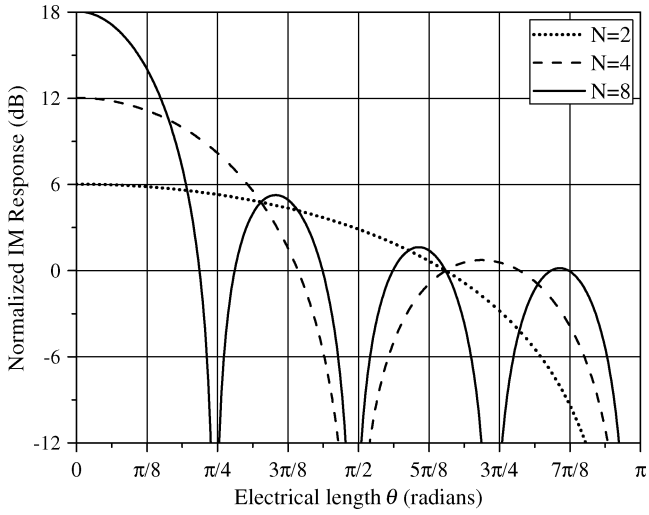

Fig. 2. Transfer function contribution from the signal summation when the optical paths are identical.

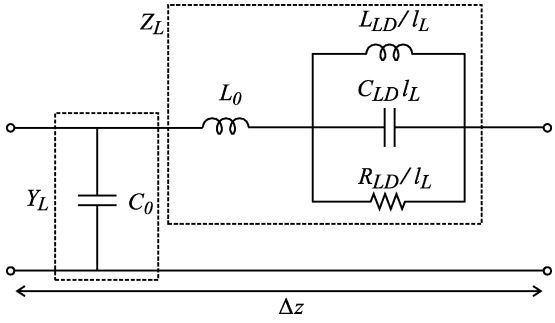

Fig. 3. Differential equivalent circuit of a TWSCL unit cell.

frequency response improves by 6 dB each time N is doubled. However, the 3-dB bandwidth decreases rapidly due to increasing phase differences between LDs as the length of the structure is increased.

3. Distributed Circuit Analysis

The preceding analysis of the TWSCL as a linear time-invariant system has allowed the transfer function to be obtained, albeit with assumptions. It is also useful to examine the TWSCL structure from the perspective of an equivalent distributed circuit, a method that has been used for distributed amplifiers [35], [36]. In Fig. 1(b), it is assumed that electrical length θ is sufficiently small to allow the LD equivalent circuit elements to be distributed across the unit cell. This is useful for analysis at relatively low frequencies but will not be valid at frequencies close to or greater than the LD resonant frequency. For simple models of distributed amplifiers, a typical distributed circuit model involves having the shunt lumped capacitance element at the gate (or drain) of the transistor distributed across the unit cell. Intuitively, this is not difficult to accept since the differential equivalent circuit of a transmission line contains shunt conductance and shunt capacitance. For the TWSCL differential circuit model, however, the LD appears as a parallel resonant circuit in series with the incremental inductance of the transmission line. Even so, the concept of distributing lumped parameters across the unit cell is still valid, but the restrictions and ramifications will be examined later. Also, the following distributed circuit analysis will be carried out with respect to the electrical characteristics only. Where the modulation response of the TWSCL is needed, the transfer function will be invoked.

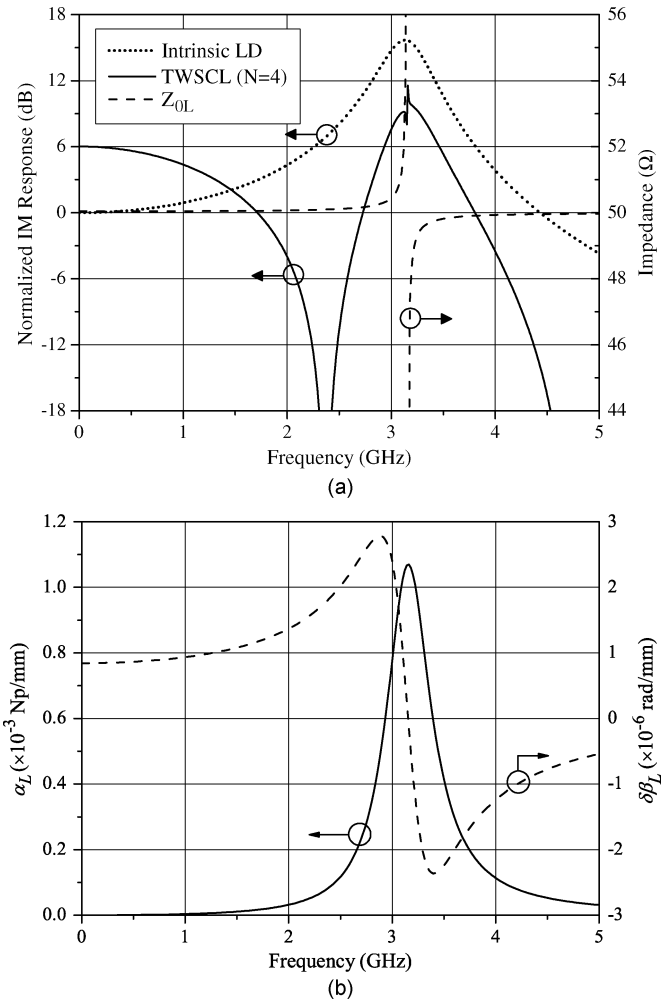

Fig. 4. (a) Approximate characteristic impedance Z_{0L} of the TWSCL and effect on magnitude of the transfer function. (b) Attenuation function and deviation from a linear phase coefficient of the TWSCL $(N = 4)$.

The distributed parameters of the equivalent TWSCL transmission line can be obtained by considering the differential circuit of the unit cell as depicted in Fig. 3. To obtain this circuit, the series impedance of the lumped parallel resonant LD model is divided by the unit cell length l_L. From Fig. 3, the distributed impedance Z_L and admittance Y_L are given by

$$Z_L = j\omega L_0 + \left(\frac{1}{j\omega L_{\mathrm{LD}}/l_L} + \frac{1}{R_{\mathrm{LD}}/l_L} + j\omega C_{\mathrm{LD}} l_L\right)^{-1}, \qquad Y_L = j\omega C_0. \tag{9}$$

As a first-order approximation the characteristic impedance is taken to be purely real, which implies a lossless differential model (i.e., the term in R_{LD} in the expression for Z_L is neglected). This is reasonable provided that the modulation frequencies are strictly less than the LD resonant frequency as will be shown later. With this caveat in mind

$$Z_{0L} = \sqrt{\frac{Z_L}{Y_L}} = \sqrt{\left(L_0 + \frac{L_{\mathrm{LD}}}{l_L}\frac{1}{1-\omega^2/\omega_{\mathrm{LD}}^2}\right)\Big/ C_0}. \tag{10}$$

One observes from the second term in the numerator of (10) an effective reduction of the inductance L_{LD}. The intrinsic LD inductance is typically several picohenries. Further division of this

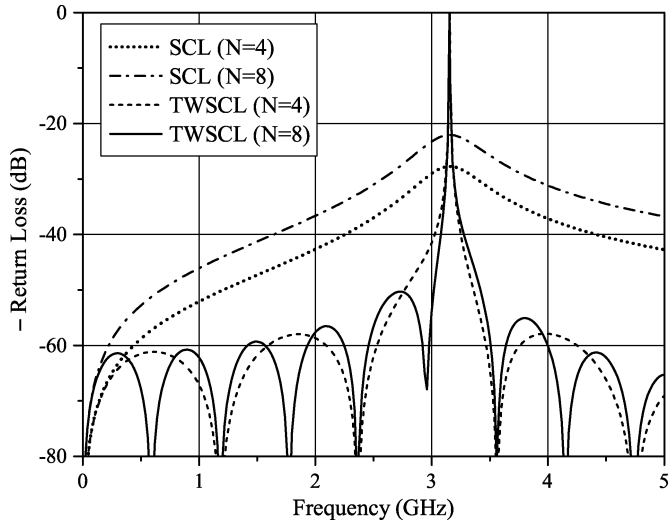

Fig. 5. Comparison of the input return loss of an SCL matched using a 50-Ω resistor with a TWSCL.

parameter by l_L means that it will be negligible relative to L_0 and hence Z_{0L} is very close to the transmission line impedance Z_0, as shown in Fig. 4(a). The figure also shows that the impedance $Z_{0L} \rightarrow \pm\infty$ as $\omega \rightarrow \omega_0$, that is the lossless approximation breaks down rapidly as ω_0 is approached. Another example shown in Fig. 4(a) is the magnitude of the transfer function where the input impedance is not taken to be ideal but calculated using (10) as a parameter.

The complex propagation coefficient, γ_L can also be obtained from $\gamma_L = \sqrt{(Z_L Y_L)} = \alpha_L + j\beta_L$ where the attenuation and phase coefficients can, respectively, be approximated by

$$\alpha_L \approx \frac{R_{\mathrm{LD}}}{2Z_0 l_L} \Bigg/ \left(1+\left(\frac{R_{\mathrm{LD}}}{\omega L_{\mathrm{LD}}}\right)^2\left(1-\frac{\omega^2}{\omega_{\mathrm{LD}}^2}\right)^2\right) \tag{11}$$

$$\beta_L \approx \omega\sqrt{L_0 C_0}\cdot\left(1+\frac{L_{\mathrm{LD}}}{2L_0 l_L}\frac{1-\omega^2/\omega_{\mathrm{LD}}^2}{\left(1-\omega^2/\omega_{\mathrm{LD}}^2\right)^2+\left(\omega L_{\mathrm{LD}}/R_{\mathrm{LD}}\right)^2}\right). \tag{12}$$

These expressions were obtained by taking a Taylor series expansion of the square root about dc and keeping the first two terms. Unlike the derivation of Z_0, the intrinsic model resistance R_{LD} is retained. From (11), the attenuation coefficient is maximum at the resonant frequency. An example of the attenuation function is shown in Fig. 4(b) for the values $R_{\mathrm{LD}} = 1.07\ \Omega$, $L_{\mathrm{LD}} = 8.9$ pH, $C_{\mathrm{LD}} = 286$ pF, $\varepsilon_{\mathrm{eff}} = 10$, $Z_0 = 50\ \Omega$, and $l_L = 10$ mm.

It is useful to note that the maximum value for the attenuation is governed by the ratio R_{LD}/Z_0 and the unit cell length. However, the latter may not be increased arbitrarily as the approximations used here are only valid when the unit cell's electrical length is short. Moreover, the result given here underestimates the attenuation since chip parasitics provide additional resistance of a few ohms. Inspection of the phase coefficient equation (12) reveals that the TWSCL distributed circuit is electrically smooth because the SRI inductance of the LD is typically 100 times smaller than L_0. The deviation, $\delta\beta_L$, from the linear phase coefficient, which is about a thousand times larger, is shown in Fig. 4(b). Therefore, there will be negligible dispersion for waves on the electrical circuit in this particular example. The input impedance of the TWSCL can now be calculated from basic transmission line theory [37]

$$Z_{\mathrm{IN}} = Z_{0L}\frac{Z_T + Z_{0L}\tanh\gamma_L N l_L}{Z_{0L} + Z_T\tanh\gamma_L N l_L} \tag{13}$$

where Z_{0L} is obtained from (10). The termination Z_T is set to 50 Ω. The input return loss is then calculated with a source impedance of 50 Ω and plotted in Fig. 5. For comparison, the return loss for

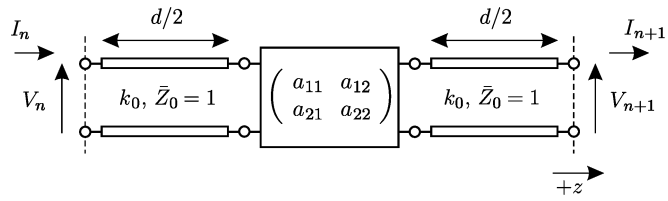

Fig. 6. Unit cell of a transmission line of length d and normalized characteristic impedance $\overline{Z_0} = 1$ loaded by a passive reciprocal two-port.

two SCLs consisting of four and eight LDs is shown. The example presented here is close to virtually ideal in terms of matching since the intrinsic LD impedance is very small. However, the SCL return loss is poorer when the cascade is longer. More importantly, the TWSCL provides relatively better matching due to the distributed effect and is less affected, in terms of the impedance magnitude, by increasing the number of LDs. In practice, the magnitude of the LD impedance will be larger due to chip and interconnection parasitics. Thus the matching performance of the SCL will not be as good as shown here, especially when the cascade is long [22].

4. Bloch Wave Analysis

The distributed circuit analysis of Section 3 breaks down close to resonance, as seen in Figs. 3 and 5. In particular, as the frequency increases, it is no longer appropriate to assume that the LD parameters are fully distributed across the length of the structure. Instead, one must analyze the TWSCL as a periodic structure [37]. There are common mathematical ideas in the analysis of periodic structures regardless of whether it is optical waves propagating through a layered dielectric, electromagnetic waves traveling on a periodically loaded transmission line or electron waves propagating through the lattice of a solid. The wave solutions in the latter are termed Bloch waves, and by analogy (following [37]), the terminology is used in the microwave domain. In [37], Collin gives the analysis of periodic structures using transmission line theory for lossless loads. To apply Collin's treatment to transmission lines periodically loaded with LDs, it needs to be generalized to include lossy loads. In the small-signal regime and neglecting the optical output, it is assumed that the LDs of a TWSCL can be considered as linear passive reciprocal two-ports.

Consider the unit cell shown in Fig. 6 consisting of the series cascade of two transmission line sections each having a normalized characteristic impedance of unity, phase coefficient of k_0 and length of $d = 2$, with a passive reciprocal two-port. From transmission line theory, the following relations can be obtained at the nth unit cell:

$$\begin{pmatrix} V_n \\ I_n \end{pmatrix} = \begin{pmatrix} t_{11} & t_{12} \\ t_{21} & t_{22} \end{pmatrix} \begin{pmatrix} V_{n+1} \\ I_{n+1} \end{pmatrix} = e^{\gamma d} \begin{pmatrix} V_{n+1} \\ I_{n+1} \end{pmatrix} \tag{14}$$

where the matrix of elements t_{xy} is the transmission matrix from the cascade of the transmission lines and the two-port network, and $\gamma = \alpha + j\beta$ is the propagation coefficient of the periodic circuit. The nontrivial solution of the matrix eigenvalue equation obtained from (14) leads to

$$\cosh\gamma d = \frac{t_{11} + t_{22}}{2} = \cos\theta + j\frac{\overline{Z}}{2}\sin\theta \tag{15}$$

where $\theta/2$ is the electrical length of the unit cell transmission lines. Expanding the right-hand side and equating real and imaginary parts gives

$$\varphi(\theta) = \cosh(\alpha d)\cos(\beta d) = \cos(\theta) - \frac{\mathrm{Im}\{\overline{Z}\}}{2}\sin(\theta) \tag{16}$$

$$\rho(\theta) = \sinh(\alpha d)\sin(\beta d) = \frac{\mathrm{Re}\{\overline{Z}\}}{2}\sin(\theta). \tag{17}$$

Squaring and combining yields

$$\frac{\varphi^2(\theta)}{\cosh^2(\alpha d)} + \frac{\rho^2(\theta)}{\sinh^2(\alpha d)} = \cos^2(\beta d) + \sin^2(\beta d) = 1 \tag{18}$$

which is solved for the intermediate variable $u = \cosh(\alpha d)$ in terms of φ and ρ

$$u_{\pm} = \frac{1}{2}\left(1+\varphi^2+\rho^2 \pm \sqrt{\left((\varphi-1)^2+\rho^2\right)\left((\varphi+1)^2+\rho^2\right)}\right). \tag{19}$$

For passive two-ports, the positive solution cannot occur; hence, the attenuation coefficient is

$$\alpha = \frac{1}{d}\cosh^{-1}(\sqrt{u_-}). \tag{20}$$

Using this result and (16) and (17), the phase coefficient can be expressed as

$$\beta = \frac{1}{d}\tan^{-1}\left(\frac{\rho}{\varphi\tanh(\alpha d)}\right). \tag{21}$$

The normalized characteristic Bloch impedance at the terminal plane of the unit cell is defined as

$$\overline{Z}_B^{\pm} = \frac{V_{n+1}}{I_{n+1}} = \frac{2t_{12}}{t_{22} - t_{11} \pm \sqrt{(t_{11}+t_{22})^2 - 4}} \tag{22}$$

where the plus and minus signs refer to waves propagating in the $+z$ and $-z$ directions (see Fig. 6), respectively. If the unit cell is symmetric, a simpler result can be obtained for $Z_B^{\pm}$, i.e.,

$$\overline{Z}_B^{\pm} = \pm\sqrt{\frac{t_{12}}{t_{21}}}. \tag{23}$$

If the load is a series impedance $\overline{Z}$, the characteristic Bloch impedance can then be written as

$$\overline{Z}_B = \sqrt{\frac{\overline{Z}(\cos k_0 d + 1) + j2\sin k_0 d}{\overline{Z}(\cos k_0 d - 1) + j2\sin k_0 d}} \approx \sqrt{1 - j\frac{\overline{Z}}{k_0 d}} \tag{24}$$

where the approximation on the right hand side of (24) assumes that the unit cell electrical length is small compared with the wavelength. Thus, subject to this assumption, it can be shown that a parallel RLC load gives rise to a characteristic impedance of

$$Z_B = \sqrt{\frac{1}{j\omega C_0}} \cdot \sqrt{j\omega L_0 + \frac{1}{\left(j\omega\frac{L_{\mathrm{LD}}}{d}\right)^{-1} + j\omega(C_{\mathrm{LD}}d) + \frac{1}{R_{\mathrm{LD}}/d}}} \tag{25}$$

which is the impedance of the differential equivalent circuit from Section 3. Furthermore, if the attenuation is small, using (16) gives an expression for the phase coefficient when the load is a parallel RLC network, that is

$$\beta_L = \omega\sqrt{L_0 C_0}\beta_0 \tag{26}$$

where

$$\beta_0 = \sqrt{1 + \frac{L_{\mathrm{LD}}}{L_0 l_L}\frac{1-\omega^2/\omega_{\mathrm{LD}}^2}{\left(1-\omega^2/\omega_{\mathrm{LD}}^2\right)^2 + (\omega L_{\mathrm{LD}}/R_{\mathrm{LD}})^2}}. \tag{27}$$

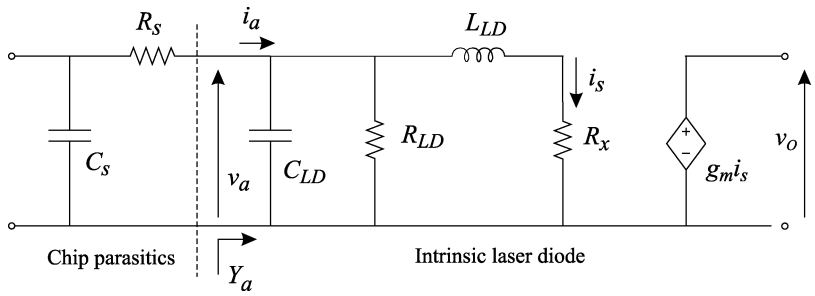

Fig. 7. Small-signal equivalent circuit model of laser diode. After [32].

The attenuation function can then be obtained using (17) as

$$\alpha_L = \frac{R_{\mathrm{LD}}}{2Z_0 l_L} \Bigg/ \left(1 + \left(\frac{R_{\mathrm{LD}}}{\omega L_{\mathrm{LD}}}\right)^2 \left(1 - \frac{\omega^2}{\omega_{\mathrm{LD}}^2}\right)^2\right) \beta_0. \tag{28}$$

Comparing these results with the corresponding expressions from Section 3 reveals that the latter are approximations of the respective expressions derived here.

Modeling the LD as a parallel RLC network is arguably a theoretical curiosity. A more practical model is to use a small-signal circuit model derived from the single-mode rate equations (see Fig. 7), including chip parasitics and a bond-wire inductance, as a periodic series load. The normalized load impedance is given by

$$\overline{Z} = \frac{1}{Z_0}\left(j\omega L_P + \frac{R_S + Z_{\mathrm{LD}}}{1 + j\omega C_S (R_S + Z_{\mathrm{LD}})}\right) \tag{29}$$

where Z_{LD} is the un-normalized intrinsic LD impedance

$$Z_{\mathrm{LD}} = \frac{R_{\mathrm{LD}}}{1 + j\omega R_{\mathrm{LD}} C_{\mathrm{LD}} \left(1 + \frac{1}{j\omega R_x C_{\mathrm{LD}} - \omega^2 L_{\mathrm{LD}} C_{\mathrm{LD}}}\right)}. \tag{30}$$

Fig. 8 shows the impact of the parasitics on the characteristic impedance, calculated using (24). This demonstrates that for typical values of the intrinsic LD parameters, the circuit parasitics have a more significant role in the impedance [39].

4.1. Impedance Matching

In a terminated periodic structure, the Bloch voltage and current wave equations can be written down in a very similar manner to the general solutions for the waves on a terminated transmission line. Given boundary conditions dictated at one end by a termination Z_t and at the other end by a source with internal impedance Z_s, the input impedance of the periodic structure can be calculated by solving the wave equations. The theoretical computation (see [37]) closely resembles the same computation for a transmission line terminated by a load. The main differences are that the line impedance is replaced by $Z_B^{\pm}$, the choice of sign determined by $\pm z$ Bloch waves, and the propagation coefficient is calculated using (20) and (21). It is assumed that the LDs are lumped elements. The computation of the TWSCL input return loss was implemented in Mathematica. Since the parasitics dominate the Bloch impedance, a simplification of the small-signal LD model was employed by assuming that the intrinsic LD impedance is approximately zero. Calculations were carried out with the line impedance and length as the main parameters. The parasitic circuit parameters were $L_p = 0.3$ pH, $C_s = 3$ pF and $R_s = 4.5\ \Omega$. Contour plots were constructed with the criterion of meeting a specified return loss under various conditions, as shown in Fig. 9. Fig. 9(a) and (b) show that broadband matching can be achieved. The regions between contour x and contour y indicate a matching bandwidth between x and y GHz. Increasing the return loss desired reduces the area of the (d, Z_0) regions that can satisfy the requirement. These plots suggest a

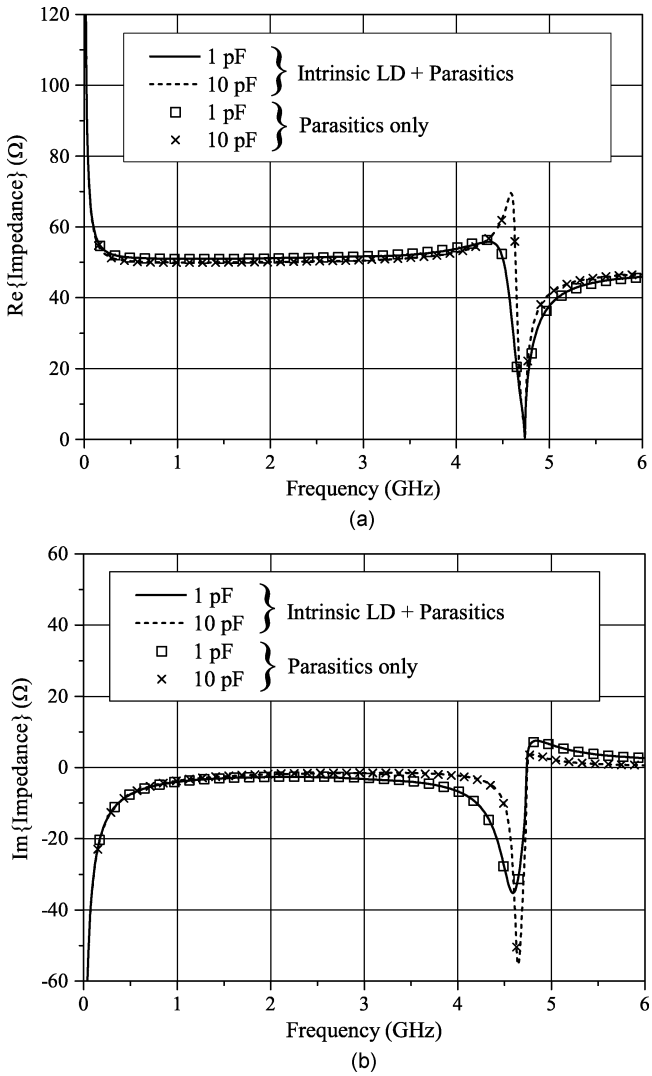

Fig. 8. Parasitics dominate the characteristic impedance of a TWSCL structure: $L_p = 0.2$ nH, $R_s = 4.5\ \Omega$, $L_{LD} = 8.9$ pH, $C_{LD} = 0.29$ nF, $R_{LD} = 1.1\ \Omega$, $R_x = 20\ m\Omega$, $Z_0 = 50\ \Omega$, and $d = 10$ mm.

maximum achievable return loss given a set of LD parameters. As this maximum is approached the contour regions continue to decrease in area. Thus, near the maximum possible return loss, the matching will be sensitive to the tolerance of the line parameters. Comparing the cascade of four against eight LDs in Fig. 9(c) and (d), shows small differences in the contours, with the area of the regions satisfying the requirement remaining roughly the same. Reducing the termination from 50 Ω to 30 Ω [see Fig. 9(e)] slightly decreases the area of the solution, while increasing it from 50 Ω to 80 Ω [see Fig. 9(f)] increases the solution area. For typical values of the chip capacitance and resistance, the impact on the input matching was found to be small. It should be noted that as $d \rightarrow 0$, i.e., as the length of the unit cell approaches zero, the LD lumped assumption breaks down. In this region, it is perhaps more appropriate to model the LD using traveling-wave rate equations [40].

4.2. GBP

The −3-dB bandwidth and GBP were calculated using the same base code used in the impedance matching program, with additional code to determine the LD terminal current. The impedance of the intrinsic LD was assumed to be negligible and ideal combining of each LD output

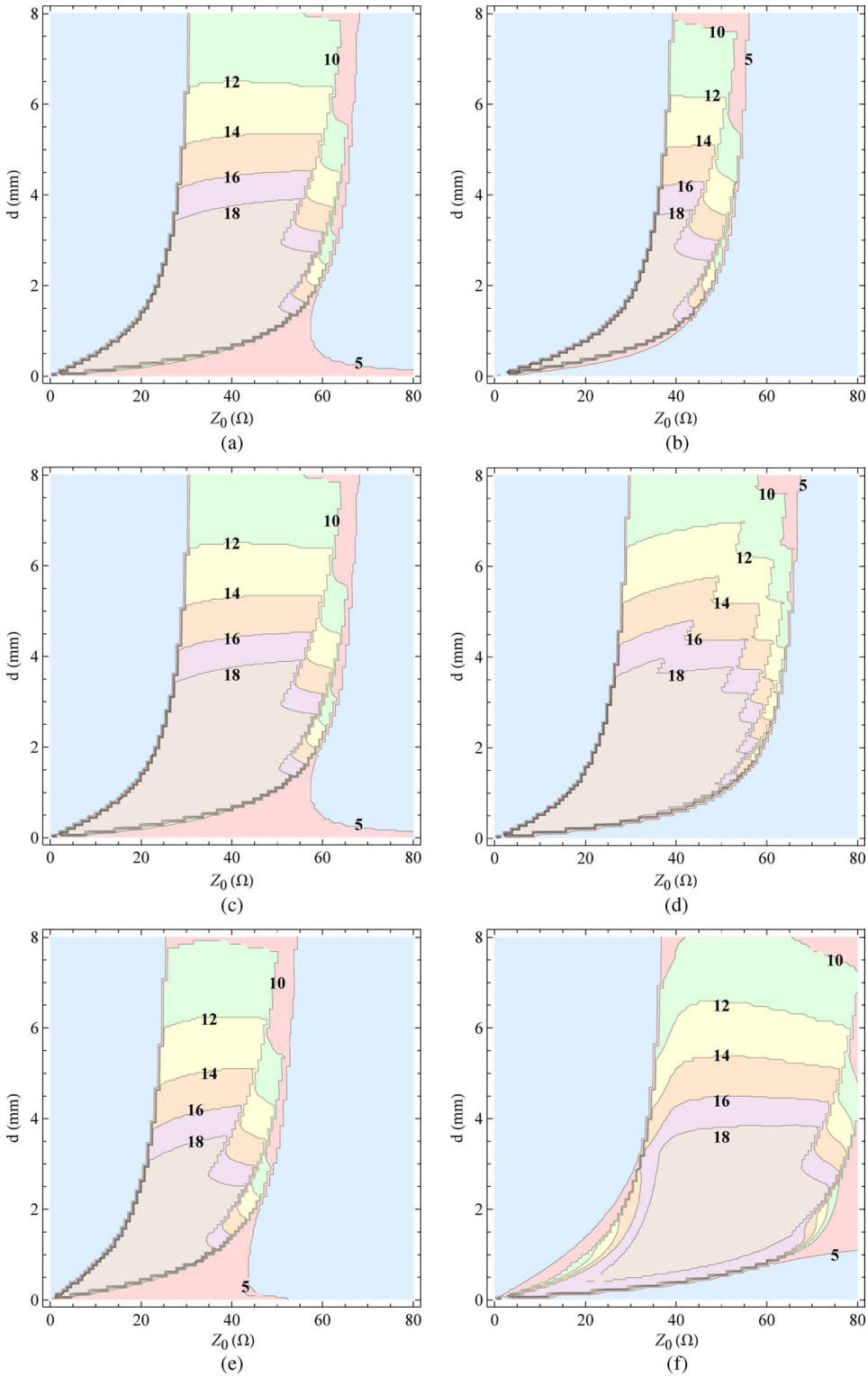

Fig. 9. Contours of return loss for a TWSCL cascade. Unless stated otherwise, the return loss specification is at least 10 dB for a TWSCL having four laser diodes and terminated by 50 Ω. The contour annotation is the maximum frequency bandwidth (from dc) that meets the specification, in gigahertz. (a) 10 dB return loss. (b) 15 dB return loss. (c) Four LDs. (d) Eight LDs. (e) $Z_t = 30\ \Omega$. (f) $Z_t = 80\ \Omega$.

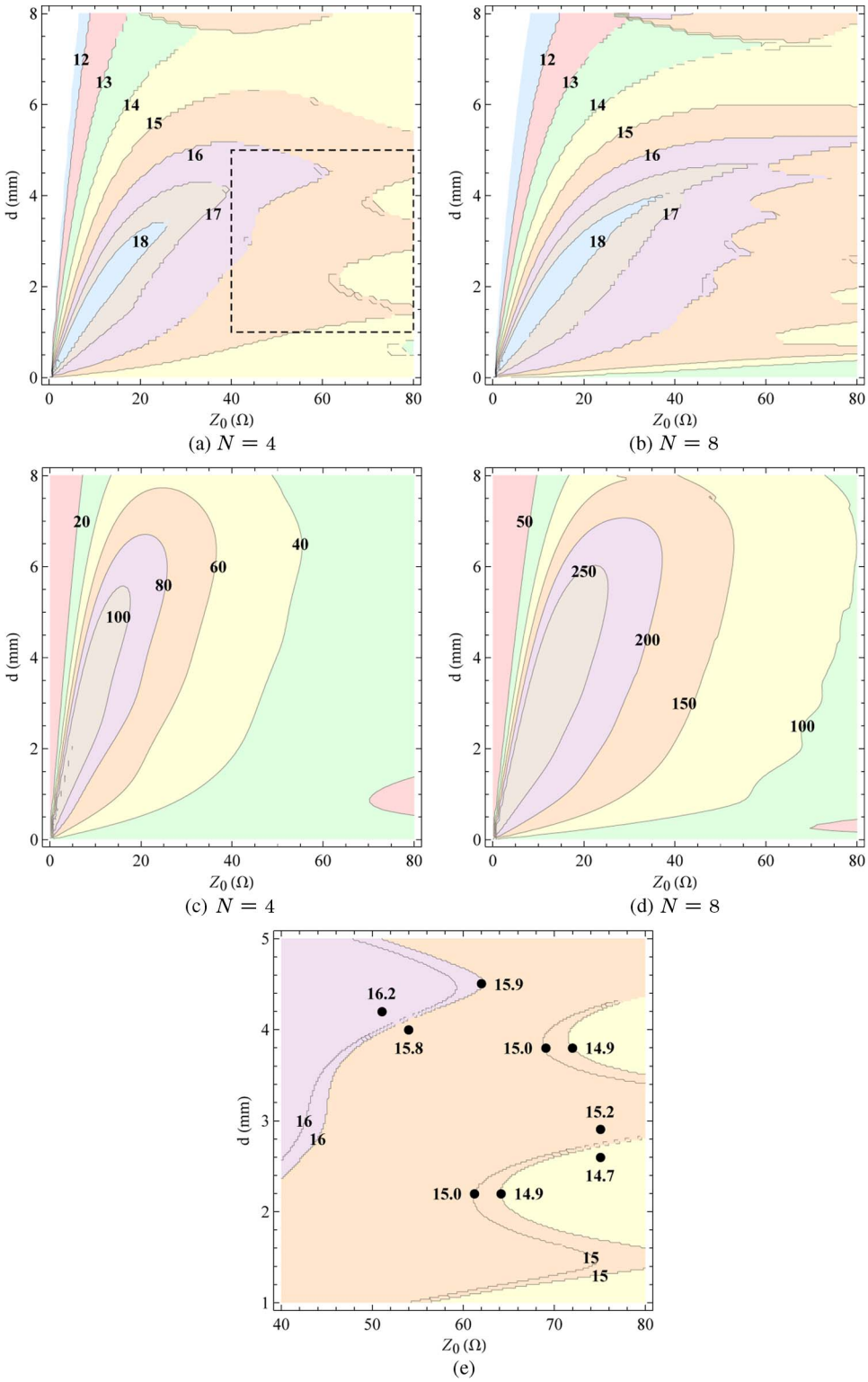

Fig. 10. (a) and (b) Small-signal bandwidth and (c) and (d) GBP for TWSCLs with four and eight laser diodes. Contours are in gigahertz. The dashed box in (a) is recomputed at higher resolution in (e), where solid circles were obtained from circuit simulation in ADS.

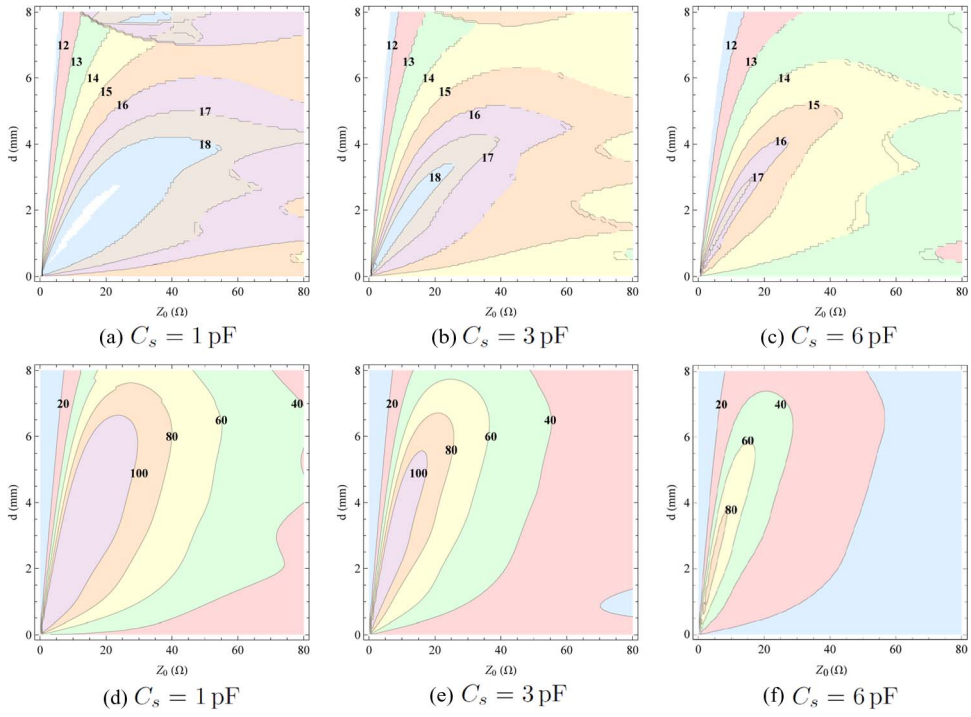

Fig. 11. Effect of varying the LD chip capacitance on the bandwidth [(a), (b), and (c)] and the gain-bandwidth product [(d), (e), and (f)].

was also assumed. The available gain, i.e., the ratio of the power delivered to the load to the available power at the TWSCL input was calculated. An ideal photodetector model converts all optical power to current with 100% efficiency. The optical power was calculated from the photon density which was in turn obtained from the product of the transimpedance of the small-signal model with the current through the inductive branch of the intrinsic LD circuit. The transimpedance constant was set to give reasonable values for the optical power. The GBP was calculated by numerically integrating the gain magnitude from dc to the -3-dB bandwidth. Contours of the TWSCL bandwidth and GBP (in gigahertz) were plotted for cascades of four and eight LDs, variations in the terminating impedance, and changes in the LD parasitics. The nominal parameters of the intrinsic LD were: $L_{\mathrm{LD}} = 1$ pH, $C_{\mathrm{LD}} = 0.2$ nF, $R_{\mathrm{LD}} = 0.7\ \Omega$, and $R_x = 10\ \mathrm{m}\Omega$. Fig. 10 shows the simulation results for TWSCLs having four and eight LDs. A bandwidth of 18 GHz can be obtained at relatively low line impedance in both cases. The maximum GBP for the longer cascade is roughly 2.5 times the four-LD version. Comparing the GBP plot with the input matching (see Fig. 9) suggests that it is not possible to simultaneously obtain good matching and maximize the GBP and that one must be traded off against the other.

A close examination of the bandwidth plots show gaps in the contour lines. This is likely a numerical rounding off issue in the Mathematica function "ListContourPlot." The bandwidth plots were calculated on a uniform "grid" of (d, Z_0) pairs, 100 points along each axis for a total of 10 000 pairs overall. The boxed area in Fig. 10(a) was recalculated and the grid "resolution" increased to 200 points along each axis, quadrupling the total computation. All calculations were load distributed over a local area network, using a rudimentary master–slave parallelization, consisting of a quad-core Intel machine with a clock rate of 3.2 GHz, a two-CPU dual-core Opteron system with a clock rate of 2 GHz, and a dual-core Intel PC at 2.4 GHz. It took approximately 9 min to calculate 10 000 points and 30 min to calculate 40 000 points, excluding postprocessing. The result of the calculations is shown in Fig. 10(e). The values marked by solid circles were obtained from circuit simulation in Agilent's ADS program. There is good agreement in the placement of the points from the circuit simulation and the calculation. The contours are more well defined and the

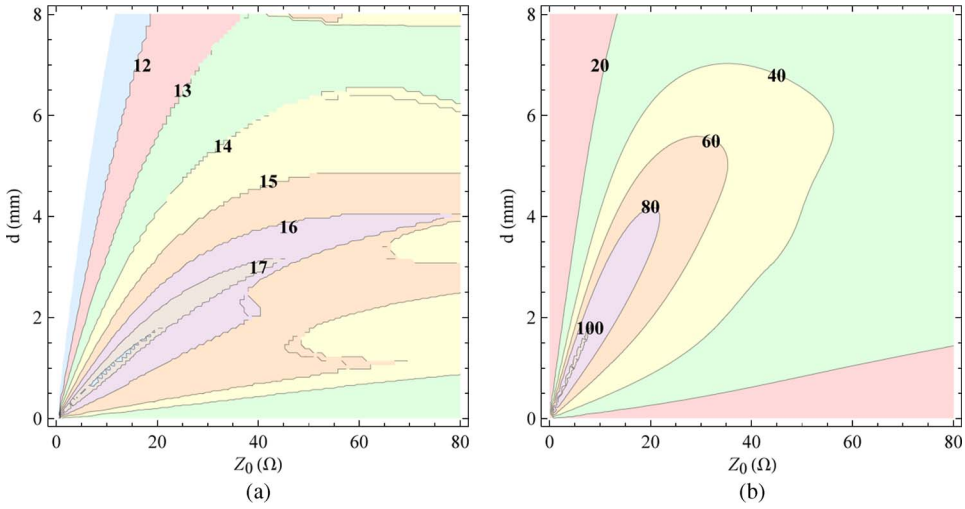

Fig. 12. Increasing the bond-wire inductance to $L_p = 0.6$ nH from $L_p = 0.3$ nH is detrimental to TWSCL performance. (a) Bandwidth. (b) GBP.

simulation results suggest that the closely spaced contours are not being properly separated by the plotting function. However, the excessive computational overhead dissuaded the use of this higher resolution. All subsequent calculations used a 2-D array of 10 000 points.

Changing the termination of the TWSCL was found to have little impact on the GBP. A more marked effect on the TWSCL performance can be seen when the parasitic LD parameters are varied. Increasing the parasitic chip capacitance reduces the bandwidth potential and the GBP of the TWSCL (see Fig. 11) as the higher admittance shunts more current away from the intrinsic LD. Doubling the bond-wire inductance from 0.3 nH to 0.6 nH (see Fig. 12) reduces potential bandwidth and GBP as the LD terminal current is decreased.

5. Conclusion

We have explained the small-signal operation of the TWSCL via three techniques: i) derivation of the intensity modulation transfer function; ii) a distributed circuit model; and iii) Bloch wave analysis of a periodically loaded transmission line for lossy loads. The first technique is useful in terms of illustrating possible link gain improvements through increasing the number (N) of LD elements and to determine the impact of different delay schemes on the overall intensity modulation response, while the second approach provides some insight into the effect of LD parameters on the electrical characteristics of the TWSCL, specifically its return loss. However, the most rigorous approach is that based on Bloch wave analysis, especially as the modulation frequency approaches the LD intrinsic resonant frequency. Through this method, we have investigated the impact of various parameters, including the number of LDs, the terminating impedance, the parasitic elements, and the transmission line unit cell length and characteristic impedance on the return loss, bandwidth, and GBP.

References

[1] A. J. Seeds and K. J. Williams, "Microwave photonics," *J. Lightw. Technol.*, vol. 24, no. 12, pp. 4628–4641, Dec. 2006.
[2] C. H. Cox, *Analog Optical Links*. Cambridge, U.K.: Cambridge Univ. Press, 2004.
[3] J. Capmany and D. Novak, "Microwave photonics combines two worlds," *Nature Photon.*, vol. 1, no. 6, pp. 319–330, Jun. 2007.
[4] S. Iezekiel, "Measurement of microwave behavior of optical links," *IEEE Microw. Mag.*, vol. 9, no. 3, pp. 100–120, Jun. 2008.
[5] R. A. Minasian, "Photonic signal processing of microwave signals," *IEEE Trans. Microw. Theory Tech.*, vol. 54, no. 2, pp. 832–846, Feb. 2006.
[6] C. H. Cox, III, E. I. Ackerman, G. E. Betts, and J. L. Prince, "Limits on the performance of RF-over-fiber links and their impact on device design," *IEEE Trans. Microw. Theory Tech.*, vol. 54, no. 2, pp. 906–920, Feb. 2006.

[7] U. Gliese, "Coherent fiber-optic links for transmission and signal processing in microwave and millimeter-wave systems," in *Proc. MWP*, Princeton, NJ, Oct. 1998, pp. 211–214.
[8] A. Ramaswamy, L. A. Johansson, J. Klamkin, H.-F. Chou, C. Sheldon, M. J. Rodwell, L. A. Coldren, and J. E. Bowers, "Integrated coherent receivers for high-linearity microwave photonic links," *J. Lightw. Technol.*, vol. 26, no. 1, pp. 209–216, Jan. 2008.
[9] E. K. Lau, X. Zhao, H.-K. Sung, D. Parekh, C. Chang-Hasnain, and M. C. Wu, "Strong optical injection-locked semiconductor lasers demonstrating >100-GHz resonance frequencies and >80-GHz intrinsic bandwidths," *Opt. Express*, vol. 16, no. 9, pp. 6609–6618, Apr. 2008.
[10] J. P. van der Ziel and W. T. Tsang, "Integrated multilayer GaAs lasers separated by tunnel junctions," *Appl. Phys. Lett.*, vol. 41, no. 6, pp. 499–501, Sep. 1982.
[11] J. C. H. Garcia, E. Rosencher, P. H. Collot, N. Luarent, J. Guyaux, B. Vinter, and J. Nagle, "Epitaxially stacked lasers with Esaki junctions: A bipolar cascade laser," *Appl. Phys. Lett.*, vol. 71, no. 26, pp. 3752–3754, Dec. 1997.
[12] W. Schmid, D. Wiedenmann, M. Grabherr, R. Jager, R. Michalzik, and K. J. Ebeling, "CW operation of diode-cascade InGaAs quantum well VCSEL," *Electron. Lett.*, vol. 34, no. 6, pp. 553–555, Mar. 1998.
[13] S. G. Patterson, G. S. Petrich, R. J. Ram, and L. A. Kolodziejski, "Continuous-wave room temperature operation of bipolar cascade laser," *Electron. Lett.*, vol. 35, no. 5, pp. 395–397, Mar. 4, 1999.
[14] J. T. Getty, O. Buchinsky, R. A. Salvatore, B. Mason, P. G. Piva, S. Charbonneau, K. S. Grabowski, and L. A. Coldren, "Monolithic series-connected 1.55 μm segmented-ridge lasers," *Electron. Lett.*, vol. 35, no. 15, pp. 1257–1258, Jul. 1999.
[15] S. G. Ayling, D. R. Wight, M. B. Allenson, K. P. Hilton, and G. W. Smith, "Novel integrated laser devices with greatly enhanced quantum efficiency and intrinsic RF matching for low loss, broad band optomicrowave applications," in *Proc. Int. Topical Meeting Microw. Photon.*, 1998, pp. 161–164.
[16] C. H. Cox, III, H. V. Roussell, R. J. Ram, and R. J. Helkey, "Broadband, directly modulated analog fibre link with positive intrinsic gain and reduced noise figure," in *Proc. Int. Topical Meeting Microw. Photon.*, 1998, pp. 157–160.
[17] F. Rana and R. J. Ram, "Photon noise and correlations in semiconductor cascade lasers," *Appl. Phys. Lett.*, vol. 76, no. 9, pp. 1083–1085, Feb. 2000.
[18] J. K. Kim, S. Nakagawa, E. Hall, and L. A. Coldren, "Near-room-temperature CW operation of electrically-pumped multiple-active-region 1.55-μm VCSELs with high differential efficiency," *Appl. Phys. Lett.*, vol. 77, no. 20, pp. 3137–3139, Nov. 2000.
[19] T. Knodl, M. Golling, A. Straub, and K. J. Ebeling, "Multi-diode cascade VCSEL with 130% differential quantum efficiency at CW room temperature operation," *Electron. Lett.*, vol. 37, no. 1, pp. 31–33, Jan. 2001.
[20] K. D. Choquette, E. Young, K. Geib, D. Serkland, A. Allerman, C. Cox, E. Ackerman, and H. Rousell, "Cascade vertical cavity surface emitting laser arrays," in *Proc. 15th IEEE LEOS*, Nov. 10–14, 2002, pp. 327–328.
[21] J. T. Getty, L. A. Johansson, E. J. Skogen, and L. A. Coldren, "1.55-μm bipolar cascade segmented ridge lasers," *IEEE J. Sel. Topics Quantum Electron.*, vol. 9, no. 5, pp. 1138–1145, Sep./Oct. 2003.
[22] J. T. Getty, E. J. Skogen, L. A. Johansson, and L. A. Coldren, "CW operation of 1.55-μm bipolar cascade laser with record differential efficiency, low threshold, and 50 Ω matching," *IEEE Photon. Technol. Lett.*, vol. 15, no. 11, pp. 1513–1515, Nov. 2003.
[23] T. Knödl, M. Golling, A. Straub, R. Jäger, R. Michalzik, and K. J. Ebeling, "Multistage bipolar cascade vertical-cavity surface-emitting lasers: Theory and experiment," *IEEE J. Sel. Topics Quantum Electron.*, vol. 9, no. 5, pp. 1406–1414, Sep./Oct. 2003.
[24] P. Modh, S. Galt, J. Gustavsson, S. Jacobsson, and A. Larsson, "Linear cascade VCSEL arrays with high differential efficiency and low differential resistance," *IEEE Photon. Technol. Lett.*, vol. 18, no. 1, pp. 100–102, Jan. 2006.
[25] W. J. Siskaninetz, J. E. Ehret, J. D. Albrecht, R. G. Bedford, T. R. Nelson, Jr., and J. A. Lott, "Gigahertz modulation of GaAs-based bipolar cascade vertical cavity surface-emitting lasers," *Opt. Lett.*, vol. 32, no. 2, pp. 136–138, Jan. 2007.
[26] F. Dross, F. Van Dijk, and P. Gallion, "Discussion on the improvement of opto-RF link properties by using a bipolar cascade laser source," *IET Optoelectronics*, vol. 1, no. 1, pp. 9–15, Feb. 2007.
[27] D. A. Tauber, R. Spickerman, R. Nagarajan, T. Reynolds, A. L. Holmes, Jr., and J. E. Bowers, "Inherent bandwidth limits in semiconductor lasers due to distributed microwave effects," *Appl. Phys. Lett.*, vol. 64, no. 13, pp. 1610–1612, Mar. 1994.
[28] B. Wu, J. B. Georges, D. M. Cutrer, and K. Y. Lau, "On distributed microwave effects in semiconductor lasers and their practical implications," *Appl. Phys. Lett.*, vol. 67, no. 4, pp. 467–469, Jul. 1995.
[29] H. H. Hashim and S. Iezekiel, "Traveling-wave semiconductor cascade laser using wavelength division multiplexing," in *Proc. IEEE Int. Topical Meeting Microw. Photon.*, Valencia, Spain, 2009, pp. 1–4.
[30] H. H. Hashim and S. Iezekiel, "Intermodulation distortion in traveling-wave semiconductor cascade lasers," in *Proc. IEEE Annu. Photon. Meeting*, Belek-Antalya, Turkey, 2009, pp. 589–590.
[31] M. Morishita, T. Ohmi, and J. Nishizawa, "Impedance characteristics of double heterostructure laser diodes," *Solid State Electron.*, vol. 22, no. 11, pp. 951–962, Nov. 1979.
[32] R. S. Tucker and D. J. Pope, "Microwave circuit models of semiconductor injection lasers," *IEEE Trans. Microw. Theory Tech.*, vol. MTT-31, no. 3, pp. 289–293, Mar. 1983.
[33] L. N. Binh, *Photonic Signal Processing: Techniques and Applications*. Boca Raton, FL: CRC, 2007.
[34] T. Wong, *Fundamentals of Distributed Amplification*, 1st ed. Norwood, MA: Artech House, 1993, pp. 1–113.
[35] D. M. Pozar, *Microwave Engineering*, 2nd ed. New York: Wiley, 1998, pp. 635–641.
[36] Y. Ayasli, R. L. Mozzi, J. L. Vorhaus, L. D. Reynolds, and R. A. Pucel, "A monolithic GaAs 1–13 GHz traveling-wave amplifier," *IEEE Trans. Microw. Theory Tech.*, vol. MTT-30, no. 7, pp. 976–981, Jul. 1982.
[37] L. Brillouin, *Wave Propagation in Periodic Structures*, 1st ed. New York: McGraw-Hill, 1946, pp. 193–226.
[38] R. E. Collin, *Foundations for Microwave Engineering*, 2nd ed. New York: McGraw-Hill, 1992, pp. 550–566.
[39] S. Weisser, I. Esquivias, P. Tasker, J. Ralston, and J. Rosenzweig, "Impedance, modulation response, and equivalent circuit of ultra-highspeed $In_{0.35}Ga_{0.65}AsGaAs$ MQW lasers with p-doping," *IEEE Photon. Technol. Lett.*, vol. 6, no. 7, pp. 782–785, Jul. 1994.
[40] K. Y. Lau and A. Yariv, "High-frequency current modulation of semiconductor injection lasers," in *Semiconductors and Semimetals*. London, U.K.: Academic, 1985, pp. 70–148.